How warm was the Last Interglacial? New model-data comparisons

Journal:	*Philosophical Transactions A*
Manuscript ID:	RSTA-2013-0097
Article Type:	Research
Date Submitted by the Author:	28-Jan-2013

Complete List of Authors:	Otto-Bliesner, Bette; National Center for Atmospheric Research, Climate and Global Dynamics Division Rosenbloom, Nan; National Center for Atmospheric Research, Climate and Global Dynamics Division Stone, Emma; University of Bristol, School of Geographical Sciences McKay, Nicholas P.; Northern Arizona University, School of Earth and Environmental Sustainability Lunt, Daniel; University of Bristol, School of Geographical Sciences Brady, Esther C.; National Center for Atmospheric Research, Climate and Global Dynamics Division Overpeck, Jonathan T.; University of Arizona, Department of Geosciences

Issue Code: Click here to find the code for your issue.:	DM1011
Subject:	Climatology < EARTH SCIENCES, Geology < EARTH SCIENCES
Keywords:	Last interglacial, Climate change, Climate modeling, Polar warmth

Abstract

A Community Climate System Model, Version 3 (CCSM3) simulation for 125ka during the Last Interglacial (LIG) is compared to two recent proxy reconstructions to evaluate surface temperature changes from modern. The dominant forcing change from modern, the orbital forcing, modified the incoming solar insolation at the top of the atmosphere, resulting in large positive anomalies in boreal summer. Greenhouse gas concentrations are similar to those of the preindustrial Holocene. CCSM3 simulates an enhanced seasonal cycle over the Northern Hemisphere continents with warming most developed during boreal summer. In addition, year-round warming over the North Atlantic is associated with a seasonal memory of sea ice retreat in CCSM3, which extends the effects of positive summer insolation anomalies on the high latitude oceans to winter months. The simulated Arctic terrestrial annual warming, though, is much less than the observational evidence, suggesting either missing feedbacks in the simulation and/or interpretation of the proxies. Over Antarctica, CCSM3 cannot reproduce the large LIG warming recorded by the Antarctic ice cores, even with simulations designed to consider observed evidence of early LIG warmth in Southern Ocean and Antarctica records and the possible disintegration of the West Antarctic Ice Sheet. Comparisons with a HadCM3 simulation indicates that sea ice is important for understanding model polar responses. Overall, the models simulate little global annual surface temperature change, while the proxy reconstructions suggest a global annual warming at LIG (as compared to the preindustrial Holocene) of ~1°C, though with possible spatial sampling biases. The CCSM3 SRES B1 (low scenario) future projections suggest high-latitude warmth similar to that reconstructed for the LIG may be exceeded before the end of this century.

1. Introduction

Since the start of the industrial age, atmospheric greenhouse gases have increased to levels that the Earth has not experienced for over at least 800,000 years. These increases have changed the Earth's energy balance with an estimated radiative forcing of 1.6 W m^{-2} [1]. Environmental changes associated with these changes in forcing are detectable and numerous, including a global warming of 0.74°C from 1906 to 2005 and a rate of sea level rise averaging 1.8 mm/year for 1961 to 2003 [1]. Projections of future surface temperature changes by 2100 AD range from 1.1 to 6.4°C depending on the emission scenario pathway followed. Uncertainties include the degree of polar amplification of temperatures, which vary among the models used for projections [2]. Yet warming of the atmosphere, oceans, and land in the polar regions have important implications for stability of the Greenland and Antarctic ice sheets, permafrost degradation and associated methane release, and sustainability of the biological diversity.

Over the last million years, the Earth's climate has oscillated between colder, glacial climates and warmer, interglacial climates. These changes were driven by the well-known orbital periods [3], which altered the latitudinal and seasonal incoming solar radiation, with resulting feedbacks of greenhouse gases and ice sheets amplifying the orbital forcing. Some of the past interglacials over the last 500 kyrs may have been warmer than today [4-6]. Understanding the forcings and feedbacks that produced interglacial warmth and the outcomes from it can help us better project the future climate of our planet. Climate model simulations allow an assessment of how well models used for projecting future climate can reproduce the evidence from past interglacials.

The Last Interglacial (LIG, from ~130-116 ka) is a useful target for model-data comparisons for several reasons. Because it is the penultimate interglacial before the Holocene, our present interglacial, more data is available to compare to models than for earlier interglacials. Ocean drilling has retrieved a large number of sediment cores for the LIG [see 6-8]. Ice cores provide records of temperature derived from stable water isotopes that extend through the LIG in Greenland [9] and the last 800 kyrs in Antarctica [10,11]. The availability of pollen records from the LIG, particularly at extratropical latitudes in the Northern Hemisphere, allows estimates of temperature owing to the close relation of plants and climate [12].

These paleoclimatic records provide geographical patterns of temperature change for comparison to climate model simulations. Early simulations with atmospheric General Circulation Models (GCMs) and idealized orbital configurations of maximum tilt and eccentricity and perihelion at June 21 simulated significantly warmer Northern Hemisphere mid- and high-latitude summers [13]. High-latitude winters were also simulated to be warmer than modern due to sea-ice feedbacks. Atmosphere Ocean General Circulation Models (AOGCMs) with orbital forcings of 125ka and 130ka confirm these patterns of seasonal warmth [14-17]. AOGCMs though have not been able to produce the warming indicated by the East Antarctic ice cores when forced by orbital forcing changes only [17,18]. Transient simulations for the LIG with intermediate complexity models [19] suggest that Arctic warming peaked early in the interglaciation because obliquity peaked earlier than precession [20], while meltwater forcing introduced to the North Atlantic can generate an early Antarctic warming [17].

In this paper we compare the CCSM3 climate model simulations for 125ka to two recent data syntheses, assess the parallels, and explore the differences. We use the model simulation to inform an interpretation of data seasonality [21-23]. Due to limitations on the absolute dating of proxy records during the LIG, both data syntheses assessed maximum warmth in the period 135-118ka and assumed this warmth was broadly synchronous in time. We include comparisons to CCSM3 simulations for 130ka and 120ka to evaluate this assumption. We also evaluate a sensitivity simulation with the West Antarctic Ice Sheet removed to test the impact of its extent being much reduced during the LIG [18,24]. We conclude with a comparison to a HadCM3 125ka simulation, which gives an indication of the robustness of the temperature responses across models, as well as a comparison to the warmth projected for the end of this century.

2. Model description, experimental design, and forcings

We use simulations from a fully-coupled, global atmosphere-land surface-ocean-sea ice general circulation model: the Community Climate System Model, Version 3 (CCSM3). Future climate predictions from this model are presented in the IPCC AR4 report [1]. The model has also been used in the Palaeoclimate Modelling Intercomparison Project (PMIP) to simulate Last Glacial Maximum and Mid-Holocene climates [25,26].

The CCSM3 was developed by the U.S. modeling community and is maintained at the National Center for Atmospheric Research (NCAR). We use the T85x1 version of CCSM3 [27] with no flux adjustments. The atmosphere model CAM3 is a three-dimensional primitive equation model solved with the spectral method in the horizontal and with 26 hybrid coordinate levels in the vertical [28]. The T85 spectral resolution corresponds to an equivalent grid spacing of approximately 1.4° in latitude and longitude. The land model CLM3 uses the same grid as the atmospheric model and includes specified but multiple land cover and plant functional types within a grid cell [29]. The ocean model is the NCAR implementation of the Parallel Ocean Program (POP), a three-dimensional primitive equation model in vertical z-coordinate [30]. The x1 ocean grid has 320 X 384 points with poles located in Greenland and Antarctica, and 40 levels extending to 5.5km depth. The ocean horizontal resolution corresponds to a nominal grid spacing of approximately 1° in latitude and longitude with greater resolution in the tropics and North Atlantic. The sea ice model uses the same horizontal grid as the ocean model. It is a dynamic-thermodynamic formulation, which includes a subgrid-scale ice thickness distribution and elastic-viscous-plastic rheology [31].

Coupled pre-PMIP3 climate simulations have been completed with the CCSM3 for preindustrial conditions (PI) and for 125ka. For the results in this paper, the CCSM3 statistics are calculated from the last 30 years of a 950-year preindustrial simulation (started from a 1990 AD control simulation) and the last 30 years of a 350-year 125ka simulation (started from a previous LIG simulation with an earlier version of the model CCSM2). Differences between the LIG and PI simulations are evaluated with the Student t-test. The CCSM3 125ka and PI simulations were run sufficiently long to minimize surface trends. Small trends, less than 0.1°C/century, are still present in the Southern Ocean. The deep ocean is still not in equilibrium with the temperatures at 2.6km depth cooling a ~0.1°C/century in both the 125ka and PI simulations.

For the 125ka and PI simulations, we assume present-day geography, Greenland and Antarctic ice sheets, and vegetation (Table 1). The greenhouse gas concentrations for

125ka: carbon dioxide (CO_2) and methane (CH_4) are estimated from ice core measurements [32]. Those for PI are set appropriate for 1870 AD (Table 1). The greenhouse gas changes result in a radiative forcing (defined as 125ka versus PI, and calculated using formulas from the 2001 IPCC report [33]) of -0.36 W m^{-2}. The solar constant in the 125ka simulation was set to 1367 W m^{-2}, the value used in the CCSM3 present-day simulation to allow comparison to previous simulations done with the earlier CCSM2 model [16]. The solar constant in the PI simulation, on the other hand, was set to 1365 W m^{-2}, as in the CCSM3 PMIP2 simulations. The net effect of the differences in the solar constant and greenhouse gas concentrations result in a net radiative forcing of -0.02 W m^{-2}.

The Earth's orbital configuration during the LIG was different than it is today and this constitutes the dominant forcing change for 125ka as compared to modern. These orbital changes are well understood and can be calculated from astronomical equations [3]. The obliquity (tilt of the Earth's axis) with a ~ 41 kyr quasi-periodicity was larger at 125ka (23.80°) than today (23.44° for 1990AD). Obliquity modulates solar insolation at high latitudes of both hemispheres. Eccentricity, with dominant periodicities of approximately 100 kyrs and 400 kyrs, was also much larger during the LIG (0.040 at 125ka as compared to 0.0167 for 1990AD). It serves to modulate the 20 kyr precessional cycle. Perihelion (closest distance of Earth to Sun) took place in late July (boreal summer) at 125ka but occurs in early January (boreal winter) in 1990 AD.

The orbital forcing modifies the incoming solar insolation at the top of the atmosphere (Fig. 1). The annual changes at 125ka as compared to today are small, less than a few W m^{-2}. Seasonal changes, on the other hand, are large, with anomalies as big as ±10 to 15% of average insolation. At 125ka, June insolation increases by more than 55 W m^{-2} at high northern latitudes and mean May-June-July insolation anomalies at 65°N are ~20% greater than in the early Holocene [23]. This increase is partially compensated during the boreal winter such that annual changes are less than 3 W m^{-2} at these latitudes. Summer insolation in the SH was reduced relative to PI.

3. Datasets

We compare the climate model results to two recent LIG data syntheses [7,8]. Both compilations are based on published records with quantitative estimates of mean annual surface temperature change. In the marine-only dataset of McKay et al. [8], seasonal anomalies are also available with the overall pattern similar to the annual anomalies. The only available synthesis over land is for annual anomalies [7].

The Turney and Jones [7] global dataset is made up of 263 published records that span the LIG and have quantitative estimates of mean annual surface temperature. Three ice core temperature estimates from $\delta^{18}O$ are included from Greenland and four from East Antarctica. Marine records of mean annual sea surface temperature (SST) include those obtained from foraminifera, radiolarian and diatom transfer functions and calibrations using Mg/Ca and Sr/Ca ratios, and alkenone unsaturation indices (i.e., $U^{k'}_{37}$). Absolute dating of LIG proxy records is difficult. Because of this, Turney and Jones average the temperature estimates across the isotopic plateau associated with the LIG in the marine and ice core records. The terrestrial mean annual surface temperature estimates are based on the original interpretations from pollen, macrofossils, and Coleoptera, taking the period of maximum warmth and assuming that this warmth is broadly synchronous with the marine and ice core plateaus. The pollen and macrofossil records are converted to quantitative temperature estimates in the original publications using a variety of methods, including modern analogue, regressions, and other inversions. Annual temperature changes are calculated from modern using the present-day mean annual temperatures at each paleosite location using the 1961-1990 CRU dataset [34]for terrestrial sites and ESRL dataset [35]for ocean sites.

The McKay et al. [8] global dataset is a compilation of 76 records from published paleoceanographic sites. The annual SST estimates are from Mg/Ca in foraminifera, alkenone unsaturation ratios $U^{k'}_{37}$, and faunal assemblage transfer functions for radiolaria, foraminifera, diatoms, and coccoliths. Only records with published age models and an average temporal resolution of 3 kyrs or better for the LIG and late Holocene were included. Because of dating uncertainties, McKay et al. average the SST estimates for a 5000-year period centered on the warmest temperatures between 135 and 118ka at each site. SST changes are calculated from the late Holocene (last 5 kyr). This compilation was additionally supplemented with the 94 CLIMAP Project LIG SST change from core-top values.

The combined datasets, which include some overlap over the oceans, give a broadly consistent global synthesis of global mean annual temperature (MAT) change (Fig. 2). Annual surface temperatures were warmer than modern at mid and high latitudes of both hemispheres. The data indicates strong warming in the northern and southern polar regions, generally greater than 4 to 5°C north of 60°N over land and ocean, and 2 to 5°C for the Antarctic ice cores. The very large warming over northern Asia and Alaska are based on pollen and plant macrofossils and may reflect a bias towards summer warming [23]. A less consistent picture emerges for temperature changes in the tropics. Coastal upwelling regions, particularly along the California coast and the African coast south of the equator, indicate warming. The rest of the tropical Atlantic Ocean was cooler during the LIG while the eastern tropical Pacific Ocean has adjacent cores suggesting warming and cooling. The data coverage is good for the Atlantic Ocean and eastern Pacific basin, but poor over the rest of the Pacific Ocean, the Indian and Southern Oceans, and in the continental interiors. The analysis of McKay et al. suggests a peak LIG global annual SST warming of 0.7±0.6°C as compared to the late Holocene. Turney and Jones suggest a peak LIG annual surface temperature warming (land+ocean) of 1.5±0.1°C compared to a 1961-1990 AD baseline, or ~1.9°C warmer than PI [35].

4. Simulated surface temperatures

4.1 Mean annual surface temperatures (MAT)

The simulated MAT change at 125ka relative to preindustrial shows significant warming at high and mid-latitudes of the NH (Fig. 3). This warming is greatest over the North Atlantic south of Greenland (in excess of 4°C) in agreement with proxy estimates of SST anomalies ranging from 2.7 to 5°C. The model also simulates warming farther north in the Greenland-Iceland-Norwegian (GIN) Seas, though a comparison with the data is less straightforward because of wide disparity among the proxy estimates of SST change. Warming over North America and Eurasia is greatest in the western portions of these continents and decreases eastward to slight warming or even slight cooling. The model simulates warmer SSTs off the coasts of California and Spain in good agreement with the data.

The model underestimates the proxy indications of warming for the far northern coastal regions of Alaska (simulated: 0.5 to 1°C versus data: 5.5 to 6.7°C) and Siberia (simulated: 1 to 2°C versus data: 7.1 to 14.8°C). A possible reason is that the models do not include vegetation feedbacks [16,suppl material, 36], which could be important in these high-latitude regions (see section 5). The simulated surface temperature anomalies at the summit of Greenland are 2.2°C as compared to NGRIP and GRIP stable water isotope estimates of annual warming of 5°C [37,38]. Some of the observed warming may be associated with reduced elevation of the central Greenland ice sheet [9,39].

CCSM3 also simulates mean annual warming over the SH subtropical landmasses of South America, Africa, and Australia, but lack of terrestrial proxies in the data syntheses for these regions does not allow evaluation of the model. Slightly cooler MAT are simulated for Antarctica in contrast to East Antarctic ice core records that indicate substantial warming of 1.5 to 4.5°C [10, 32, 40,41]. Simulated cooler MAT over North Africa and southern Asia are consistent with the simulated enhanced summer monsoons. Previous modeling studies [42] and paleorecords [43-45] also confirm the relationship between increased seasonality of the insolation in the Northern Hemisphere and expansion/intensification of these monsoon systems.

Simulated SST changes south of 30°N are small, generally within ±1°C of the preindustrial control simulation. The data, on the other hand, show more regionally variable anomalies. Coastal upwelling regions record much warmer SSTs not simulated by the model. Coastal upwelling regions are difficult for climate models to resolve and simulate well [46]. The reconstructions show SST cooling in excess of 2°C over the tropical Atlantic and Indian Oceans, though with limited data coverage in the latter.

Simulated changes in these ocean basins are of the correct sign but underestimate the magnitude of the observed cooling. For the Southern Ocean, the data suggest larger SST anomalies than the model, although with significant regional heterogeneity.

CCSM3 shows strong polar amplification of MAT north of ~45°N with approximately similar warming over the ice-free oceans and continents (Fig. 4). This is associated with a seasonal memory of sea ice retreat in CCSM3 that extends the effects of positive summer insolation anomalies on the high latitude oceans to winter months, affecting the North Atlantic, Arctic Ocean, and adjacent continents. Over mid-latitude continental regions, the strong summer warming dominates the annual average. South of 45°N, CCSM3 simulates zonally averaged MAT close to zero or slightly negative, with stronger continental cooling at subtropical northern latitudes associated with the African and Asian monsoons (Fig. 4).

While the proxy data suggests significant regional heterogeneity in the MAT change in the tropics and SH extratropics, the simulated response in CCSM3 is relatively uniform with no change to weak annual surface cooling at the locations of the data (Fig. 5). The proxy data suggest an average annual warming in the tropics (30°N-30°S) of ~0.3°C and at SH extratropical latitudes (30-90°S) of ~1.2°C, while CCSM3 simulates weak annual cooling of ~0.3-0.5°C in both regions (Table 2). The proxy data also indicates that the average annual warming over the continents was about twice that over the oceans in the tropics, a feature that CCSM3 does not capture (Table 2).

CCSM3 warms the NH extratropical (30-90°N) continents more than oceans, with simulated warming at the paleo-data locations ~1.0°C over the continents and ~0.5°C over the oceans (Table 2), though with much more regional heterogeneity in the simulated SST anomalies than terrestrial MAT anomalies (Fig. 5). The proxy data, on the other hand, suggest similar and larger annual warming of ~1.7°C for the terrestrial and ocean proxies. The full-grid averages from CCSM3 also show ~0.5°C more warming over the NH extratropical continents than oceans, suggesting that the lack of contrast in the data is not a reflection of the uneven data distribution.

Globally, a simple point-by-point average of the combined proxy reconstructions indicate an annual warming of 0.98°C, with the continents warming by 1.67°C and the oceans warming by 0.76°C. CCSM3 simulates no change of mean annual surface temperatures at 125ka as compared to PI (Table 2). Simulated terrestrial temperatures are globally warmer by 0.92°C when sampled at the proxy locations but show no change when averaged over all model land points. The terrestrial reconstructions are strongly biased toward middle and high latitudes, with no data included in these reconstructions in the monsoon regions in which CCSM3 simulates cooling. These results suggest that the spatial sampling of the reconstructions could introduce a strong bias in our perception of the LIG: the model can simulate warming at terrestrial proxy sites, on average, and at the same time simulate no average change in the "true" model global temperatures.

4.2 Seasonality of model response

Uncertainties exist in the reconstructions in the seasonality of biological proxies, which may be biased systematically towards specific seasons. Terrestrial quantitative reconstructions are often derived from sediments indicating a change in the geographical ranges of specific plants. The biotic dominance of high-latitude vegetation is influenced by temperature, growing season length, and moisture availability [47]. Seasonality is well constrained for Europe but less so for other regions [15,23]. The primary SST proxies are also sensitive to changes in seasonality [48,49]. SSTs derived from foraminifera Mg/Ca are known to reflect the calcification temperature of the species, which is best represented by the warm season conditions [50]. Environmental preferences of alkenone-producing algae may bias their proxy data estimates towards warmer temperatures, particularly in regions affected by both upwelling and open ocean conditions [51]. Locally their signal can also be strongly seasonal [52,53].

The simulated surface temperatures for 125ka show a strong seasonality of the surface temperature response (Fig. 6) consistent with the solar insolation anomalies (Fig.1). The boreal summer (JJA) warming is larger and more extensive over the NH landmasses than in the annual mean. Poleward of ~30°N, surface temperature anomalies are greater than 2°C over almost all of North America, Eurasia and Greenland, and exceed 5°C over the interiors of Europe, Asia and North America. In Siberia along the Arctic coast, simulated JJA surface temperature anomalies are 2 to 3°C greater than the annual anomalies but only 0.5 to 1°C greater in northern Alaska. In both regions, the JJA simulation shows better correspondence with the MAT reconstruction but still underestimates the proxy indications of very strong LIG MAT warming (Fig. 7). The SH continental regions located at tropical and subtropical latitudes also show enhanced warming in JJA. This is not unexpected as the positive JJA insolation anomalies extend into the tropics and SH. Antarctica shows warming in JJA in CCSM3. The simulated JJA surface temperature anomalies compare much better to the calibrated MAT data estimates over the NH extratropics than do the simulated MAT anomalies though CCSM3 cannot capture the large warming indicated by some terrestrial proxies (Fig. 7). Over the SH extratropics and tropics, the simulated JJA surface temperature changes are only modestly warmer than the simulated MAT changes (not shown).

The austral summer (DJF) simulated surface temperature anomalies are cooler in many regions, with less correspondence with the MAT-calibrated data (Figs. 6 and 7). Only over high northern latitudes are there substantial warm anomalies. These warm anomalies occur over the North Atlantic and to a lesser extent over Canada and Europe. They cannot be explained by local insolation; the DJF insolation anomalies at 125ka as compared to PI are negative at these latitudes. Rather they reflect the seasonal memory of surface temperature to the reduced sea ice and snow extent associated with the boreal summer insolation anomalies. Over northern Eurasia the simulated warming (though not significant) agrees with the expectation from proxy records of warmer winters at LIG than PI [12] but is underestimated in terms of magnitude or eastward extent. The colder SSTs simulated in the subtropical Indian Ocean in austral summer agree better with the proxy records. The lack of any improved agreement between the simulations and the data in upwelling regions suggests that seasonality is not an important consideration for the data-model mismatch.

4.3 Early, Middle, and Late LIG Simulations

Because of difficulties in absolute dating for the LIG, both data syntheses assess maximum warmth (135-118ka) and assumed this warmth was broadly synchronous in time. The seasonal and latitudinal natures of the insolation anomalies, though, change throughout the LIG. The obliquity reached a maximum of 24.24° at 130ka, remained relatively high at 23.80° at 125ka, and decreased to 23.01° at 120ka. Obliquity affects both seasonal contrasts and annual solar insolation, with the largest anomalies at high latitudes of both hemispheres. Annual insolation anomalies as compared to present reach close to 6 W m^{-2} at the poles for 130ka, remain positive but decrease to ~3 W m^{-2} for 125ka, and become a negative forcing annually at high latitudes for 120ka. Perihelion shifted from early May at 130ka to late July at 125ka to mid-September at 120ka, with important impacts on NH insolation. Seasonal changes in insolation associated with precessional forcing are strong during the entire LIG because of the large eccentricity throughout the LIG.

The orbital changes result in seasonal and latitudinal changes in insolation that evolve over the LIG (Fig. 1). At 130ka, the largest positive insolation anomalies in the NH occur in May and June and exceed 50 W m^{-2} from the North Pole to NH subtropical latitudes. By 120ka, the positive NH insolation anomalies have shifted to August and September and are much weaker.

Greenhouse gas concentrations used in the CCSM3 simulations are different for the three LIG time periods, contributing an additional radiative forcing of about 0.6 W m^{-2} at 130ka as compared to 125ka, or potentially ~0.4°C of global annual mean warming. It should be noted that the GHG concentrations used for 130ka are higher than the Dome C reconstruction followed in the PMIP3 LIG protocols [54]. Rather the CCSM3 130ka simulation is more appropriate for 128ka, which had June insolation anomalies similar to 130ka and atmospheric CO_2 and CH_4 measurements suggesting concentrations of 287 ppmv and 724 ppbv, respectively. Differences in the radiative forcings associated with modest changes in the greenhouse gas concentrations between 125ka and 120ka are small.

Globally CCSM3 is warmer at 130ka than 125ka (Tables 2 and 3). CCSM3 exhibits larger warming at 130ka than 125ka over the North Atlantic Ocean, Ellesmere Island, and Greenland (Figs. 3 and 8). The summit of Greenland warms by 3 to 3.5°C at 130ka as compared to PI, but still less than the 5°C warming indicated by the GRIP and NGRIP ice cores. The simulated greater warming at 130ka than 125ka for the eastern Canadian Arctic is consistent with evidence that the transition into the LIG was rapid, with peak summer warmth early in the LIG [23]. Warming extends farther eastward over the mid and high latitude continental regions of North America and Eurasia at 130ka than 125ka, improving but still underestimating the proxy evidence of surface temperature changes. Overall, the NH extratropics warm by 1.04°C at 130ka (as compared to 0.76°C at 125ka) in CCSM3 when sampled at the proxy locations, and 0.71°C at 130ka (as compared to 0.27°C at 125ka) when averaged for the full-grid (Tables 2 and 3),

The Antarctic surface temperature anomalies change from a slight cooling at 125ka to a slight warming at 130ka, but still cannot explain observed warming of the ice cores. Early LIG warmth in the Southern Ocean and Antarctic is consistent with East Antarctic ice core and Southern Ocean marine records [10,55]. SH extratropical and tropical simulated cooling is significantly reduced in the 130ka simulation as compared to the 125ka simulation, but both regions remain cooler than PI.

Late in the interglaciation at 120ka, the solar insolation anomalies associated with orbital changes result in simulated MAT similar to PI, with anomalies generally less than ±1°C and not significantly different than the PI control. Globally, the MAT change simulated by CCSM3 is +0.10°C at 130ka with significant warming at mid and high latitudes in the NH and some warming over Antarctica, -0.16°C at 125ka with significant warming at mid and high latitudes in the NH but strong cooling in NH monsoon regions, and -0.14°C at 120ka with little significant temperature change anywhere as compared to PI.

4.4 Vegetation and polar ice sheets

A possible explanation of model-data mismatches in some regions is that not all appropriate changes in the boundary conditions have been considered in the design of the experiments. The LIG simulations with CCSM3 assumed modern vegetation. Northern Alaska and northern Siberia are covered with tundra in these simulations. The pollen and macrofossil evidence for the LIG indicates boreal forests extending to the Arctic Ocean coastline everywhere except in Alaska and central Canada [56,57]. Boreal forests have a lower albedo than tundra and can also partially mask snow allowing for more absorption of incoming solar radiation and warming. Deciduous broad-leaf forests can also contribute to greenhouse warming due to enhanced transpiration of water vapor to the atmosphere [58]. Some of the underestimation of proxy-inferred warming may therefore be a consequence of not including vegetation feedbacks. Previous modeling of the LIG has shown that the feedback between vegetation and climate can enhance the warming at high latitudes [36,59].

Global sea level was likely 4 to 9 m higher during the LIG relative to present day [16,18,60,61]. A sea level rise of up to 4 m during this time interval has been attributed to some Greenland ice sheet and other Arctic ice fields melting in combination with ocean thermal expansion [8,16]. A Greenland ice sheet contribution above 4 m is discredited by evidence of the presence of ice in the summit cores dating to before the LIG as well as

Greenland ice sheet simulations that show if the ice sheet is completely removed, warming is an additional 10°C in disagreement with Greenland ice records [16]. Any sea-level rise above ~4 m during the LIG must then have come from the West Antarctic Ice Sheet [18] and possibly the East Antarctic Ice Sheet. WAIS is largely grounded below sea level. The WAIS plays a role in buttressing the ice sheet and is particularly sensitive to ocean temperatures and circulation. Large WAIS glaciers near the grounding line show large basal melt rates as ocean waters bathing the edges of these glaciers warm[62]. Ice sheet/ice shelf models for Antarctica demonstrate brief but dramatic interglacial retreats of the WAIS, taking one to a few thousand years, for sub-ice melting of 2 m yr^{-1} under the shelf interior [63]. Benthic foraminifera data from cores in the North Atlantic and Southern Ocean and climate simulations indicate that warm SST in the North Atlantic could have been transported to Circumpolar Deep Water around Antarctica [64]. Direct geological evidence for a retreat of this ice sheet though remains equivocal.

A possible explanation then for the LIG simulation mismatches as compared to the Antarctic ice cores is the assumption of the presence of the WAIS in the model design. To test this sensitivity, we removed the WAIS in the CCSM3 130ka simulation replacing it with ocean of depths up to 2000m. Additional significant warming is restricted to Antarctica in this simulation. CCSM3 warms the region of the WAIS by more than 10°C (Fig. 9). It also enhances the MAT warming over East Antarctica but only by a few tenths °C, still greatly underestimating the warming indicated by the ice cores. Simulations with HadCM3 [17] suggest that in addition to the WAIS retreat, freshwater input to the North Atlantic from the Laurentide and Eurasian ice sheets during the termination is needed to produce MAT warming that is consistent with the ice core data. This is consistent with evidence of persistent iceberg melting at high northern latitudes at the beginning of the LIG [55].

5. Robustness of the CCSM3 response

Simulations for the LIG are now part of PMIP3 [54], (https://pmip3.lsce.ipsl.fr/wiki/doku.php/pmip3:design:li:final). A simulation for 125ka has been completed with HadCM3 allowing us to a compare the response between CCSM3 and HadCM3.

The HadCM3 model was developed at the Hadley Centre for Climate Prediction and Research [65] and similar to CCSM3 it does not include flux corrections [66]. The atmosphere and ocean models are grid-point, primitive equation models. The resolutions of the atmospheric and land components are 3.75° in longitude by 2.5° in latitude, with 19 vertical levels in the atmosphere. The resolution of the ocean model is 1.25° by 1.25° with 20 levels in the vertical. The land surface scheme is MOSES 2.1, and the sea ice model uses a simple thermodynamic scheme and contains parameterizations of ice concentration [67] and ice drift and leads [68].

The CCSM3 and HadCM3 simulations were performed independently by each group so the experimental designs are similar but not identical, as they will be in the more formal model intercomparison project. For the 125ka and PI simulations, both models assume 125ka orbital forcing and present-day geography, Greenland and Antarctic ice sheets, and vegetation. The solar constant and greenhouse gas concentrations are slightly different for each model, but result in very similar net radiative forcing (-0.02 W m^{-2} for CCSM3 and +0.01 W m^{-2} for HadCM3). The climate sensitivities for a doubling of CO_2 are roughly comparable, being 2.7°C for CCSM3 and 3.2°C for HadCM3. The HadCM3 statistics are calculated from the last 50 years of a 550-year 125ka simulation, itself started from a preindustrial simulation of over 1000 years in length. HadCM3 was run sufficiently long to eliminate significant surface trends though trends in the deep ocean are still present.

Globally, HadCM3 simulates a warmer mean annual climate than CCSM3, with global mean annual temperature change as compared to the PI of +0.14°C for HadCM3 and -0.16°C for CCSM3, as calculated on the model grids (Tables 2 and 4). Calculated only at the data locations, HadCM3 simulates a global warming for 125ka of 0.27°C versus 0.10°C for CCSM3. The annual warming in both models is significantly less than the value of 0.98°C calculated from the combined reconstructions.

Robust features simulated by both of the models are the warming over central North America, Europe, South Africa, and Australia, and the cooling extending from North Africa to India and Southeast Asia (Figs. 3 and 10). The models disagree in their responses over Greenland and the North Atlantic, with the HadCM3 model simulating little MAT change, and CCSM3 better reproducing the large warming indicated by the reconstructions. Neither model can simulate the strong warming suggested by terrestrial data along the coastal Arctic Ocean. For the SH extratropics, HadCM3 simulates MAT ~0.5 to 1°C warmer than CCSM3, with the warming over East Antarctica simulated by HadCM3 agreeing in sign with the ice core data. However, HadCM3 cannot reproduce the 1.5 to 4.5°C MAT warming reconstructed from the East Antarctic ice cores. In the tropics, both models simulate only small MAT changes and neither can reproduce the much warmer SSTs in the coastal upwelling regions.

CCSM3 and HadCM3 differ markedly in the magnitude and even sign of polar amplification of MAT. CCSM3 shows strong polar amplification of MAT north of ~45°N over the oceans and continents (Fig. 4). South of 45°N, CCSM3 simulates zonally averaged MAT close to zero or slightly negative. HadCM3 exhibits much reduced polar amplification of the MAT and a more symmetric response with small warming at both poles. Differences between the two models may be related to their sea ice sensitivities (Figs. 3 and 10). Both models simulate strong warming at mid- to high-latitudes of the NH in JJA (not shown) consistent with the positive insolation anomalies but only CCSM3 retains memory of this warming in the North Atlantic and adjacent land regions. HadCM3 with less winter (DJF) sea ice south of Greenland at PI shows less sensitivity. In the SH, HadCM3 has less sea ice off East Antarctica than CCSM3 (white areas in Figs. 3 and 10) allowing the nearby Southern Ocean and East Antarctica to warm in response to the small positive anomalies in austral winter and spring. These results are consistent with the contrasting Arctic and Antarctic sea ice extent sensitivities in the late 20th century simulations in these two models (Arzel et al., 2006).

6. Summary and implications

CCSM3 simulations for the Last Interglacial (LIG, ~130-116ka) are compared to the two recent data syntheses of Turney and Jones [7] and McKay et al. [8]. The dominant forcing change for the LIG are the large seasonal changes in the incoming solar radiation associated with orbital forcing. The model responds with substantial annual warming at 125ka for high and mid-latitudes of the NH although underestimates the proxy indications of this warming. Over Antarctica, the model simulates cooling as compared to large LIG warming recorded by the Antarctic ice cores. CCSM3 simulates an enhanced seasonal cycle over the high-latitude continents of both hemispheres with simulated JJA warming in better correspondence with the reconstructed annual temperature changes. The observed warming was not likely globally synchronous, with the Antarctic ice cores and records from the Southern Ocean indicating early LIG warmth [10,55]. CCSM3 shows better agreement with the Southern Hemisphere records when forced with 130ka insolation anomalies than the simulation for 125ka, though the simulated warming is small. Further assessment of the seasonality of the proxy records and improvements in dating of proxy records, when possible, will be important for further assessing how well models can simulate the feedbacks in response to orbital forcing.

Some of the model-data discrepancy may be associated with the experimental design, with CCSM3 adopting present-day vegetation and polar ice sheets, boundary conditions that data and previous sensitivity simulations indicate may explain a portion of the data-model differences. A CCSM3 sensitivity simulation with the removal of the West Antarctic Ice Sheet provides additional local warming over Antarctica but still not enough to explain the ice core records. Simulations with HadCM3 [17] suggest that in addition to the WAIS retreat, freshwater input to the North Atlantic from the Laurentide and Eurasian ice sheets during the termination is needed to produce Antarctic warming that is consistent with the ice core data. A bipolar response is consistent with evidence of persistent iceberg melting at high northern latitudes at the beginning of the LIG [55].

The main series of simulations presented in this paper are from one model, CCSM3. A similar experiment for 125ka has been completed with HadCM3. This allows an assessment of robustness of the CCSM3 simulation. Both model simulations suggest little global annual surface temperature change at 125ka as compared to preindustrial, when averages are computed for the full model grids. On the other hand, both show small global warming when averaged over the data locations. Neither simulates a global warming of ~1°C suggested by a simple averaging of the proxy data, although this proxy estimate may be influenced by the lack of good spatial coverage of the data. CCSM3 and HadCM3 differ markedly in the magnitude and even sign of polar amplification of MAT, a feature influenced by their sea ice sensitivities. CCSM3 with a strong sensitivity of NH sea ice [69] simulates strong Arctic warming. HadCM3 exhibits much reduced polar amplification of the Arctic MAT and a more symmetric response with small warming at both poles. The similarities and differences in the responses in CCSM3 and HadCM3 point to the need for the LIG model intercomparison project now implemented within PMIP3 [54].

It is interesting to consider the polar warmth indicated by the Turney and Jones [7] and McKay et al. [8] reconstructions in comparison to future projection simulations completed by CCSM3 and included in the IPCC AR4 WG1 [70]. The global surface annual warming projected by CCSM3 for the first few decades of the 21st century for the different SRES scenarios track each other closely. The low estimate climate change scenario (SRES B1) peaks in emissions in the mid-21st century with GHG concentrations starting to level off in the second half of this century. By the end of the 21st century, CCSM3 projects a global mean annual warming of 0.9°C for the SRES B1 scenario [70], comparable to that of the LIG reconstructions, with greater warming at high latitudes than low latitudes (Fig. 11). East Antarctica and much of the North Atlantic have warmed up to surface temperatures comparable to that of the LIG proxy records. The SRES B1 warming over Greenland is less than the LIG warmth, though, as for the CCSM3 LIG simulations, the CCSM3 future projections fix the Greenland ice sheet heights and extent at present-day. Differences in the primary forcings, orbital insolation changes for the LIG versus GHG concentrations in the SRES projections, give different seasonal responses. While the 125ka CCSM3 simulation shows the largest warming in JJA, the SRES B1 future projection simulation has the greatest high latitude warming during the respective winters of the two hemispheres. As such, it would be wrong to consider the LIG as an exact 'analogue' for future climate change.

In summary, there is no clear answer to the question posed in the title "How warm was the Last Interglacial?" Our results show model-data inconsistencies that are not fully understood. The models' sensitivity to the forcings may be too small. Our interpretation of the reconstructed climate parameters may not adequately incorporate seasonal and depth effects and age uncertainties. The implications for future warming scenarios require progress in resolving these inconsistencies between the model simulations and data reconstructions of past interglacials.

Acknowledgements

The CCSM project is supported by the U.S. National Science Foundation (NSF) and the Office of Science (BER) of the U.S. Department of Energy. NCAR is sponsored by NSF. This research was enabled by the computing resources of the Climate Simulation Laboratory. E. Stone is funded by the EU project Past4Future. This is Past4Future contribution no 33. The research leading to these results has received funding from the

European Union's Seventh Framework programme (FP7/2007-2013) under grant agreement no 243908, "Past4Future. Climate change - Learning from the past climate".

References

1. Solomon, S., Qin, D., Manning, M., Chen, Z., Marquis, M., Averyt, K.B., 2007. *Climate Change, 2007 The Physical Science Basis. Contribution of Working Group I to the Fourth Assessment Report of the Intergovernmental Panel on Climate Change.* Cambridge University Press.
2. Meehl G. A. et al, 2007 *Global Climate Projections*. In: Solomon S, D. Qin, M. Manning, Z. Chen, M. Marquis, K.B. Averyt, M. Tignor and H.L. Miller (ed) *Climate Change 2007 The Physical Science Basis. Contribution of Working Group I to the Fourth Assessment Report of the Intergovernmental Panel on Climate Change*. Cambridge University Press, Cambridge, United Kingdom and New York, NY, USA, 747-845.
3. Berger A. L., 1978 Long-term variations of caloric insolation resulting from the earth's orbital elements. *Quaternary Res* **9**, 139-167.
4. Tzedakis, P. C., D. Raynaud, J. F. McManus, A. Berger, V. Brovkin, and T. Kiefer, 2009 Interglacial diversity. *Nat Geosci* **2,** 751-755.
5. Tzedakis, P. C., 2010 The MIS 11 – MIS 1 analogy, southern European vegetation, atmospheric methane and the "early anthropogenic hypothesis." *Clim. Past* **6**, 131-144.
6. Lang, N. & E. W. Wolff, 2011 Interglacial and glacial variability from the last 800 ka in marine, ice and terrestrial archives. *Clim. Past* **7**, 361-380.
7. Turney, C. S. M. & R. T. Jones, 2010 Does the Agulhas Current amplify global temperatures during super-interglacials? *J Quaternary Sci* **25,** 839-843.
8. McKay, N. P., J. T. Overpeck, and B. L. Otto-Bliesner, 2011 The role of ocean thermal expansion in Last Interglacial sea level rise. *Geophy Res Lett* **38**. (DOI:10.1029/2011GL048280.)
9. Masson-Delmotte, V., Braconnot, P., Hoffmann, G., Jouzel, J., Kageyama, M., Landais, A., Lejeune, Q., Risi, C., Sime, L., Sjolte, J., Swingedouw, D. and Vinther, B., 2011 Sensitivity of interglacial Greenland temperature and $\delta^{18}O$: ice core data, orbital and increased CO_2 climate simulations. *Clim. Past* **7**, 1041-1059.
10. Jouzel J., Masson-Delmotte V., Cattani O., Dreyfus G., Falourd S., Hoffmann G., Minster B., Nouet J., Barnola J. M., Chappellaz J., Fischer H., Gallet J. C., Johnsen

S., Leuenberger M., Loulergue L., Luethi D., Oerter H., Parrenin F., Raisbeck G., Raynaud D., Schilt A., Schwander J., Selmo E., Souchez R., Spahni R., Stauffer B., Steffensen J. P., Stenni B., Stocker T. F., Tison J. L., Werner M., Wolff E. W., 2007 Orbital and millennial Antarctic climate variability over the past 800,000 years. *Science* **317**, 793 - 796.

11. Stenni, B., Masson-Delmotte, V., Selmo, E., Oerter, H., Meyer, H., Röthlisberger, R., Jouzel, J., Cattani, O., Falourd, S., Fischer, H., Hoffmann, G., Iacumin, P., Johnsen, S. J., Minster, B. and Udisti, R., 2010 The deuterium excess records of EPICA Dome C and Dronning Maud Land ice cores (East 52 Antarctica). *Quaternary Sci Rev* **29**, 146-159.
12. Velichko, A. A., O. K. Borisova, and E. M. Zelikson, 2008 Paradoxes of the Last Interglacial climate: reconstructions of the northern Eurasia climate based on palaeofloristic data. *Boreas* **37**, 1-19.
13. Harrison, S. P., J. E. Kutzbach, I. C. Prentice, P. J. Behling, and M. T. Sykes, 1995 The response of Northern Hemisphere extratropical climate and vegetation to orbitally induced changes in insolation during the last interglacation. *Quaternary Res* **43**, 174-184.
14. Montoya, M., H. von Storch, and T. J. Crowley, 2000 Climate simulation for 125 kyr BP with a coupled ocean-atmosphere general circulation model. *J Climate* **13,** 1057-1072.
15. Kaspar, F. N. Kuhl, U. Cubasch, and T. Litt, 2005 A model-data comparison of European temperatures in the Eemian interglacial. *Geophys Res Lett* **21**. (DOI:10.1029/2005GL022456.)
16. Otto-Bliesner, B. L., S. J. Marshall, J. T. Overpeck, G. H. Miller, A. X. Hu, and C. L. I. P. Mem, 2006 Simulating arctic climate warmth and icefield retreat in the last interglaciation. *Science* **311**, 1751-1753.
17. Holden, P. B., N. R. Edwards, E. W. Wolff, N. J. Lang, J. S. Singarayer, P. J. Valdes, and T. F. Stocker, 2010 Interhemispheric coupling, the West Antarctic Ice Sheet and warm Antarctic interglacials. *Clim. Past* **6,** 431-443.

18. Overpeck, J. T., B. L. Otto-Bliesner, G. H. Miller, D. R. Muhs, R. B. Alley, and J. T. Kiehl, 2006 Paleoclimatic evidence for future ice-sheet instability and rapid sea-level rise. *Science* **311**, 1747-1750.

19. Bakker, P., E. J. Stone, S. Charbit, M. Gröger, U. Krebs-Kanzow, S. P. Ritz, V. Varma, S. Khon, D. J. Lunt, U. Mikolajewicz, M. Prange, H. Renssen, B. Schneider, and M. Schulz, 2012 Last interglacial temperature evolution – a model inter-comparison. *Clim Past Discuss* **8**, 4663-4699.

20. Crowley, T. J. & K.-Y. Kim, 1994 Milankovitch forcing of the Last Interglacial sea level. *Science* **265**, 1566-1568.

21. Elderfield, H. & Ganssen, G., 2000 Past temperature and $\delta^{18}O$ of surface ocean waters inferred from foraminiferal Mg/Ca ratios. *Nature* **405**, 442.

22. Conte, M. H., Sicre, M.-A., Ruhlemann, C., Weber, J. C., Schulte, S., Schulz-Bull, D., and Blanz, T., 2006 Global temperature calibration of the alkenone unsaturation index (UK'37) in surface waters and comparison with surface sediments. *Geochem Geophy Geosys* **7**. (DOI:10.1029/2005gc001054.)

23. CAPE Last Interglacial Project Members, 2006 Last Interglacial Arctic warmth confirms polar amplification of climate change. *Quaternary Sci Rev* **25**, 1383-1400.

24. Scherer, R. P., A. Aldahan, S. Tulaczyk, G. Possnert, H. Engelhardt, and B. Kamb, 1998 Pleistocene collapse of the West Antarctic Ice Sheet. *Science* **281**, 82-85.

25. Otto-Bliesner, B. L., E. C. Brady, G. Clauzet, R. Tomas, S. Levis, and Z. Kothavala, 2006 Last Glacial Maximum and Holocene climate in CCSM3. *J Climate* **19**, 2526-2544.

26. Braconnot, P., Otto-Bliesner, B., Harrison, S., Joussaume, S., Peterchmitt, J.-Y., Abe-Ouchi, A., Crucifix, M., Driesschaert, E., Fichefet, T., Hewitt, C. D., Kageyama, M., Kitoh, A., Laîné, A., Loutre, M.-F., Marti, O., Merkel, U., Ramstein, G., Valdes, P., Weber, S. L., Yu, Y., Zhao, Y., 2007 Results of PMIP2 coupled simulations of the mid-Holocene and last glacial maximum? Part 1: experiments and large-scale features. *Clim Past* **3**, 261–277.

27. Collins, W. D., Collins, W. D., M. Blackmon, C. M. Bitz, G. B. Bonan, C. S. Bretherton, J. A. Carton, P. Chang, S. C. Doney, J. J. Hack, J. T. Kiehl, T.

Henderson, W. G. Large, D. McKenna, B. D. Santer, and R. D. Smith,, 2006 The Community Climate System Model version 3 (CCSM3). *J Climate* **19**, 2122-2143.

28. Collins, W. D., P. J. Rasch, B. A. Boville, J. J. Hack, J. R. McCaa, D. L. Williamson, B. Briegleb, C. M. Bitz, S.-J. Lin, and M. Zhang, 2006 The formulation and atmospheric simulation of the Community Atmosphere Model: CAM3. *J Climate* **19**, 2144-2161.
29. Dickinson, R. E., K. W. Oleson, G. B. Bonan, F. Hoffman, P. Thorton, M. Vertenstein, Z.-L. Yang, and X. Zeng, 2006 The Community Land Model and its climate statistics as a component of the Community Climate System Model. *J Climate* **19**, 2302-2324.
30. Gent, P. R., F. O. Bryan, G. Danabasoglu, and K. Lindsay, 2006 Ocean chlorofluorocarbon and heat uptake during the 20th century in the CCSM3. *J Climate* **19**, 2366-2381.
31. Briegleb, B. P., C. M. Bitz, E. C. Hunke, W. H. Lipscomb, M. M. Holland, J. L. Schramm, and R. E. Moritz, 2004 *Scientific description of the sea ice component in the Community Climate System Model, Version 3*. NCAR Technical Note, NCAR/TN-463+STR, 70 pp.
32. Petit J. R., Jouzel J., Raynaud D., Barkov N. I., Barnola J. M., Basile I., Bender M., Chappellaz J., Davisk M., Delaygue G., Delmotte M., Kotlyakov V. M,. Legrand M., Lipenkov V. Y., Lorius C., Pe´pin L., Ritz C., Saltzman E., Stievenard M., 1999 Climate and atmospheric history of the past 420,000 years from the Vostok ice core, Antarctica. *Nature* **399**, 429-436.
33. Ramaswamy, V., and Co-authors, 2001 *Radiative forcing of climate change. Climate Change 2001: The Scientific Basis.* J.T. Houghton et al., Eds, Cambridge University Press, 349-416.
34. New M., Hulme M., Jones P. 1999 Representing twentieth-century space–time climate variability. Part I. Development of a 1961–90 mean monthly terrestrial climatology. *J Climate* **12**, 829–856.
35. Smith T. M, & R. W. Reynolds, 2005 A global merged land–air–sea surface temperature reconstruction based on historical observations (1880–1997). *J Climate* **18**, 2021–2036.

36. Crucifix, M. & Loutre, M.F., 2002 Transient simulations over the last interglacial period (126-115 kyr BP): feedback and forcing analysis *Clim Dynam* **19**, 419-433
37. Johnsen S. J, Dahl-Jensen D., Gundestrup N., Steffensen J. P., Clausen H. B., Miller H., Masson-Delmotte V., Sveinbjörnsdottir A. E., White J., 2001 Oxygen isotope and palaeotemperature records from six Greenland ice-core stations: Camp Century, Dye-3, GRIP, GISP2, Renland and NorthGRIP. *J Quaternary Sci* **16**, 299-307.
38. North Greenland Ice Core Project Members, 2004 High-resolution record of Northern Hemisphere climate extending into the last interglacial period. *Nature* **431**, 147-151.
39. Raynaud, D., J. A. Chappellaz, C. Ritz, and P. Matinerie, 1997 Air content along the Greenland Ice Core project: A record of surface climate parameters and elevation in central Greenland. *J Geophys* Res **102**, 26607-26614.
40. EPICA Community Members. 2006 One-to-one coupling of glacial climate variability in Greenland and Antarctica *Nature* **444**, 195-198.
41. Kawamura, K., Parrenin F., Lisiecki L., Uemura R., Vimeux F., Severinghaus J. P., Hutterli M. A., Nakazawa T., Aoki S., Jouzel J., Raymo M. E., Matsumoto K., Nakata H., Motoyama H., Fujita S., Goto-Azuma K., Fujii Y., Watanabe O., 2007 Northern Hemisphere forcing of climatic cycles in Antarctica over the past 360,000 years. *Nature* **448**, 912-916.
42. Braconnot, P., C. Marzin, L. Gregoire, E. Mosquet, and O. Marti, 2009 Monsoon response to changes in Earth's orbital parameters: comparisons between simulations of the Eemian and of the Holocene. *Clim Past* **4**, 281-294.
43. Gaven, E., Hillaire-Marcel, C. and Petite-Maire, N., 1981 A Pleistocene lacustrine episode in southeastern Libya. *Nature* **290**, 131-133.
44. Miller, G. H., Wendorf, F., Ernst, R., Schild, R., Close, A. E., Friedman, and Schwarcz, H. P., 1991 Dating lacustrine episodes in the eastern Sahara by the epimerization ofisoleucine in Ostrich eggshells. *Palaeogeog Palaeoclim Palaeoecol* **84**, 175-189.
45. Szabo, B. J., Haynes, C. V., and Maxwell, T. A., 1995 Ages of Quaternary pluvial episodes determined by uranium-seriesand radiocarbon dating of lacustrine deposits of Eastern Sahara. *Palaeogeog Palaeoclim Palaeoecol* **113**, 227-242.

46. Otto-Bliesner, B. L. et al., 2009 A comparison of PMIP2 model simulations and the MARGO proxy reconstruction for tropical sea surface temperatures at last glacial maximum. *Clim Dynam* **32**, 799-815.

47. Kaplan, J. O. et al., 2003 Climate change and Arctic ecosystems: 2. Modeling, paleodata-model comparisons, and future projections. *J Geophys Res* **108**. (DOI:10.1029/2002JD002559.)

48. Lorenz, S. J., J. Kim, N. Rimbu, R. R. Schneider, and G. Lohmann, 2006 Orbitally driven insolation forcing on Holocene climate trends: Evidence from alkenone data and climate modeling. *Paleoceanography* **21**. (DOI:10.1029/2005PA001152.)

49. Lohmann, G., M. Pfeiffer, T. Laepple, G. Leduc, and J.-H. Kim, 2012 A model-data comparison of the Holocene global sea surface temperature evolution. *Clim Past Discuss* **8**, 1005-1056.

50. Barker S., Cacho I., Benway H., Tachikawa K., 2005 Planktonic foraminiferal Mg/Ca as a proxy for past oceanic temperatures: a methodological overview and data compilation for the Last Glacial Maximum. *Quaternary Sci Rev* **24**, 821-834.

51. Niebler H.-S., Arz H. W., Donner B., Mulitza S., Patzold J., Wefer G., 2003 Sea surface temperatures in the equatorial and South Atlantic Ocean during the Last Glacial Maximum (23-19 ka). *Paleoceanography* **18**. (DOI:1010.1029/2003PA000902.)

52. Conte M. H., Weber J. C,, Ralph N,, 1998 Episodic particle flux in the deep Sargasso Sea: an organic geochemical assessment. *Deep-Sea Res Pt1* **45**, 1819-1841.

53. Mueller P. J, & Fischer G., 2001 A 4-year sediment trap record of alkenones from the filamentous upwelling region off Cape Blanc, NW Africa and a comparison with distributions in underlying sediments. *Deep-Sea Res Pt1* **48**, 1877-1903.

54. Lunt, D. J., A. Abe-Ouchi, P. Bakker, A. Berger, P. Braconnot, S. Charbit, N. Fischer, N. Herold, J. H. Jungclaus, V. C. Khon, U. Krebs-Kanzow, G. Lohmann, B. Otto-Bliesner, W. Park, M. Pfeiffer, M. Prange, R. Rachmayani, H. Renssen, N. Rosenbloom, B. Schneider, E. J. Stone, K. Takahashi, W. Wei, and Q. Yin, 2012 A multi-model assessment of last interglacial temperatures. *Clim Past Discuss* **8**, 3657-3691.

55. Govin, A., Braconnot, P., Capron, E., Cortijo, E., Duplessy, J. C., Jansen, E., Labeyrie, L., Landais, A., Marti, O., Michel, E., Mosquet, E., Risebrobakken, B., Swingedouw, D. and Waelbroeck, C., 2012 Persistent influence of ice sheet melting on high northern latitude climate during the early Last Interglacial. *Clim Past* **8**, 483-507.

56. Lozhkin, A. V. & Anderson, P. M., 1995 The last interglaciation of northeast Siberia. *Quaternary Res* **43**, 147–158.

57. Edwards, M. E., Hamilton, T. D., Elias, S. A., Bigelow, N. H., Krumhardt, A. P., 2003 Interglacial extension of the boreal forest limit in the Noatak Valley, northwest Alaska: Evidence from an exhumed rivercut bluff and debris apron. *Arctic Antarctic Alpine Res* **35**, 460–468.

58. Swann, A. L., Fung, I. Y., Levis, S., Bonan, G. B., and Doney, S. C., 2010 Changes in Arctic vegetation amplify high-latitude warming through the greenhouse effect *Proc Nat Acad Sci* **107,** 1295-1300.

59. Schurgers, G., Mikolajewicz, U., Gröger, M., Maier-Reimer, E., Vizcaino, M. and Winguth, A., 2007 The effect of land surface changes on Eemian climate. *Clim Dynam* **29**, 357-373.

60. Dutton, A. & K. Lambeck, 2012 Ice volume and sea level during the Last Interglacial. *Science* **337**, 216-219.

61. Kopp, R. E., Simons, F. J., Mitrovica, J. X., Maloof, A. C. and Oppenheimer, M., 2009 Probabilistic assessment of sea level during the last interglacial stage. *Nature* **462**, 863-868.

62. Rignot, E. & S. S. Jacobs, 2002 Rapid bottom melting widespread near Antarctic ice sheet grounding lines. *Science* **296**, 2020-2023.

63. Pollard, D. & R. M. DeConto, 2009 Modelling West Antarctic ice sheet growth and collapse through the past five million years. *Nature* **458**, 329-333.

64. Duplessy, J. C., D. M. Roche, and M. Kageyama, 2007 The deep ocean during the last interglacial period. *Science* **316**, 89-91.

65. Gordon, C., Cooper, C., Senior, C. A., Banks, H., Gregory, J. M., Johns, T. C., Mitchell, J. F. B.,Wood, R. A., 2000 The simulation of SST, sea ice extents and

ocean heat transports in a version of the Hadley Centre coupled model without flux adjustments. *Clim Dynam* **16**, 147–168.

66. Gregory, J. M. & Mitchell, J.F.B., 1997 The climate response to CO_2 of the Hadley Centre coupled AOGCM with and without flux adjustment. *Geophys Res Lett* **24**, 1943–1946.

67. Hibler, W. D., 1979 A dynamic thermodynamic sea ice model. *J Phys Oceanogr* **9**, 815–846.

68. Cattle, H., & Crossley, J., 1995 Modelling Arctic climate change. *Philos T R Soc S-A* **352**, 201–213.

69. Arzel, O., T. Fichefet, and H. Goosse, 2006 Sea ice evolution over the 20th and 21st centuries as simulated by current AOGCMs. *Ocean Model* **12**, 401-415.

70. Meehl, G .A., W. M. Washington, B. D. Santer, W. D. Collins, J. M. Arblaster, A. Hu, D. M. Lawrence, H. Teng, L. E. Buja and W. G. Strand Jr, 2006 Climate change projections for the 21st century and climate change commitment in the CCSM3. *J Climate* **19**, 2597-2616.

Table 1. Forcings and boundary conditions used in CCSM3 simulations

	130ka	125ka	120ka	PI (1870)
Geography	Modern	Modern	Modern	Modern
Ice sheets	Modern	Modern	Modern	Modern
Vegetation	Modern	Modern	Modern	Modern
CO_2 (ppmv)	300[1]	273	272	289
CH_4 (ppbv)	720[1]	642	570	901
N_2O (ppbv)[2]	311	311	311	281
Solar constant (W m^{-2})[2]	1367	1367	1367	1365
Orbital	130ka	125ka	120ka	1990

[1] CO_2 and CH_4 concentrations at 130ka represent peak overshoot values occurring 128-129ka on the EDC age scale. See text for more discussion.

[2] Solar constant and N_2O concentrations in LIG simulations set to present-day.

Table 2. Area-weighted global and regional mean 125ka minus PI annual surface temperature difference (^{o}C) comparison of proxy averages to CCSM3 model at the proxy locations[1] and for full model grid.

125ka	Land (^{o}C)			Ocean (^{o}C)			Land + Ocean (^{o}C)		
	Proxy	CCSM @proxy	Full-grid	Proxy	CCSM @proxy	Full-grid	Proxy	CCSM @proxy	Full-grid
Global	1.67	0.92	-0.05	0.76	-0.14	-0.21	0.98	0.10	-0.16
Tropics (30^{o}N-30^{o}S)	0.71	-0.34	-0.44	0.32	-0.31	-0.26	0.33	-0.31	-0.31
NH-extra (30^{o}N-90^{o}N)	1.68	1.01	0.49	1.75	0.52	0.05	1.71	0.76	0.27
SH-extra (30^{o}S-90^{o}S)	2.25	-0.72	-0.55	1.11	-0.41	-0.27	1.22	-0.43	-0.30

[1] Because the model grid is much finer than the proxy data grids, the model output is first averaged over a representative box at the proxy data locations (CCSM@proxy), which is either 2^{o}lat. x 2^{o}long. for the terrestrial proxy data grid, or 5^{o}lat. x 5^{o}long. for the SST proxy. The 2m reference height air temperature from the model is used over land to compare to the land proxy mean annual temperature (MAT). Over the open ocean region, the surface temperature is used to compare to the SST proxy data. To obtain an estimate of SST under sea ice, the minimum ocean freezing temperature of -1.8^{o}C is used. For comparison to the averages estimated over the proxy locations, the simulated regional mean temperature differences computed on the full model grid over the land and ocean domains is shown.

Table 3. Area-weighted global and regional mean 130ka minus PI annual surface temperature difference (^{o}C) comparison of proxy averages to CCSM3 model at the proxy locations and for full model grid. See Table 2 legend for description of calculation.

130ka	Land (^{o}C)			Ocean (^{o}C)			Land + Ocean (^{o}C)		
	Proxy	CCSM @proxy	Full-grid	Proxy	CCSM @proxy	Full-grid	Proxy	CCSM @proxy	Full-grid
Global	1.67	1.27	0.36	0.76	0.02	-0.02	0.98	0.31	0.10
Tropics (30^{o}N-30^{o}S)	0.71	0.46	-0.18	0.32	-0.18	-0.13	0.33	-0.17	-0.15
NH-extra (30^{o}N-90^{o}N)	1.68	1.34	0.98	1.75	0.71	0.36	1.71	1.04	0.71
SH-extra (30^{o}S-90^{o}S)	2.25	-0.24	0.09	1.11	-0.18	-0.05	1.22	-0.18	-0.04

Table 4. Area-weighted global and regional mean 125ka minus PI annual surface temperature difference (^{o}C) comparison of proxy averages to HadCM3 model at the proxy locations and for full model grid. See Table 2 legend for description of calculation.

125ka	Land (^{o}C)			Ocean (^{o}C)			Land + Ocean (^{o}C)		
	Proxy	HadCM @proxy	Full-grid	Proxy	HadCM @proxy	Full-grid	Proxy	HadCM @proxy	Full-grid
Global	1.67	1.09	0.23	0.76	0.03	0.10	0.98	0.27	0.14
Tropics (30^{o}N-30^{o}S)	0.71	-0.23	-0.19	0.32	-0.01	0.01	0.33	-0.002	-0.05
NH-extra (30^{o}N-90^{o}N)	1.68	1.13	0.58	1.75	0.05	0.21	1.71	0.62	0.39
SH-extra (30^{o}S-90^{o}S)	2.25	0.94	0.58	1.11	0.18	0.22	1.22	0.20	0.27

Figure legends

Fig. 1. Latitude-month insolation anomalies (W m^{-2}) for 130ka, 125ka, and 120ka as compared to Preindustrial (PI), assuming a fixed-day calendar.

Fig. 2. Reconstructed mean annual surface temperature (MAT) change for LIG from modern as reconstructed by Turney and Jones (2010) and McKay et al. (2011). See text for description of methods.

Fig. 3. CCSM3 simulated mean annual surface temperature change for 125ka minus Preindustrial overlain by reconstructed MAT changes. The surface temperatures are limited to the minimum ocean freezing temperature of -1.8°C over the ocean and ice covered regions to compare to the SST proxy data. White regions indicate sea ice in both the 125ka and PI simulations. Differences significant at less than 95% using the Student t-test are stippled.

Fig. 4. Zonal-average plots for CCSM3 simulated surface temperature changes over the oceans (SST), land (TS, surface temperature), and land plus ocean (MAT) for 125ka minus Preindustrial.

Fig. 5. Scatter plots for CCSM3 simulated vs reconstructed MAT change for 125ka minus Preindustrial for NH extratropics, tropics, and SH extratropics. Blue dots denote ocean points and green dots denote land points.

Fig. 6. As in Figure 3 for CCSM3 simulated DJF (top) and JJA (bottom) surface temperature changes for 125ka minus Preindustrial. White regions and shading as in Figure 3. Seasonal averages use a fixed-day calendar.

Fig. 7. Scatter plots for CCSM3 simulated Annual (black), JJA (red) and DJF (blue) surface temperature change for 125ka minus Preindustrial versus reconstructed MAT for NH extratropics. Seasonal averages use a fixed-day calendar.

Fig. 8. As in Figure 3 for CCSM3 130ka and 120ka simulations as compared to preindustrial simulation. White regions and shading as in Figure 3.

Fig. 9. As in Figure 3 for 130ka with the removal of the WAIS (replaced by ocean with depths up to 2000 meters)/ White regions and shading as in Figure 3.

Fig. 10. HadCM3 simulated mean annual surface temperature change for 125ka minus Preindustrial overlain by reconstructed MAT changes. White regions indicate sea ice in both the 125ka and PI simulations. Differences significant at less than 95% using the Student t-test are stippled.

Fig. 11. CCSM3 simulated mean annual, December-January-February, and June-July-August surface temperature change for 2080-2099 minus 1980-1999 in the SRES B1 low estimate climate change scenario The annual surface changes in the top panel are overlain with the reconstructed LIG MAT changes. White regions indicate sea ice in both the simulated results for the last two decades of the 20^{th} and 21^{st} centuries.

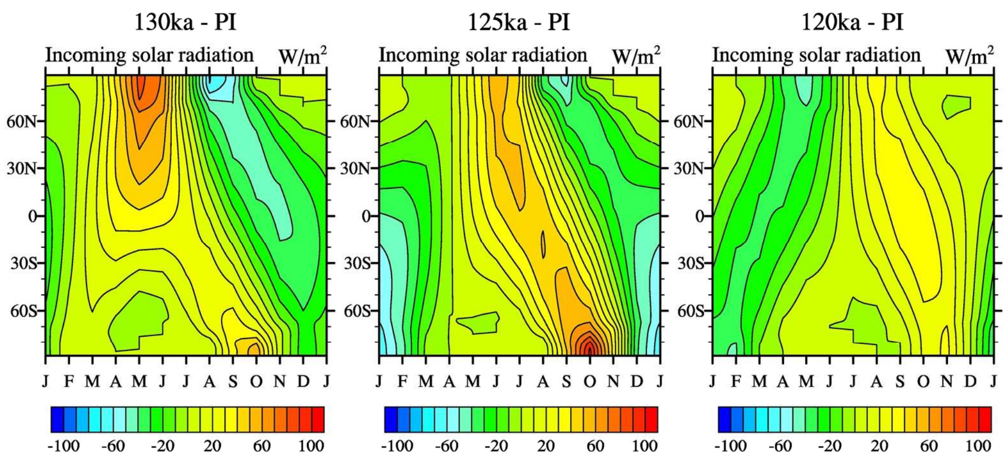

176x176mm (300 x 300 DPI)

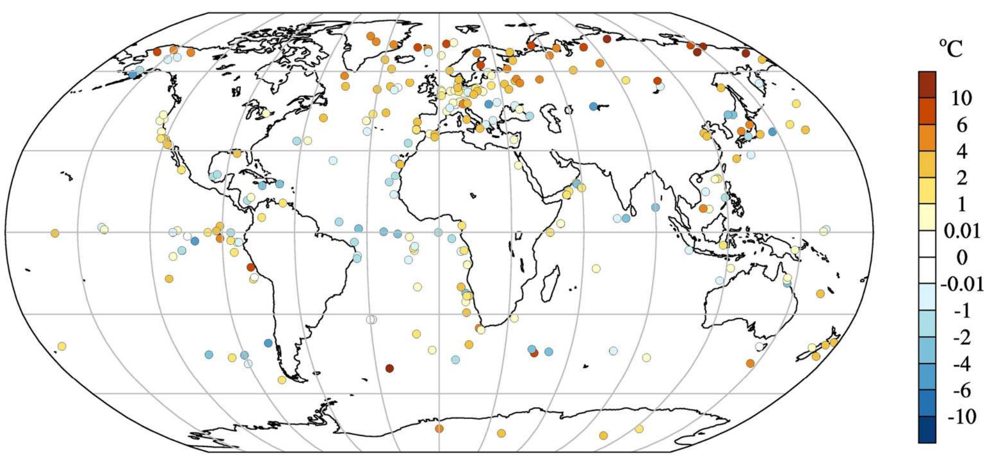

170x170mm (300 x 300 DPI)

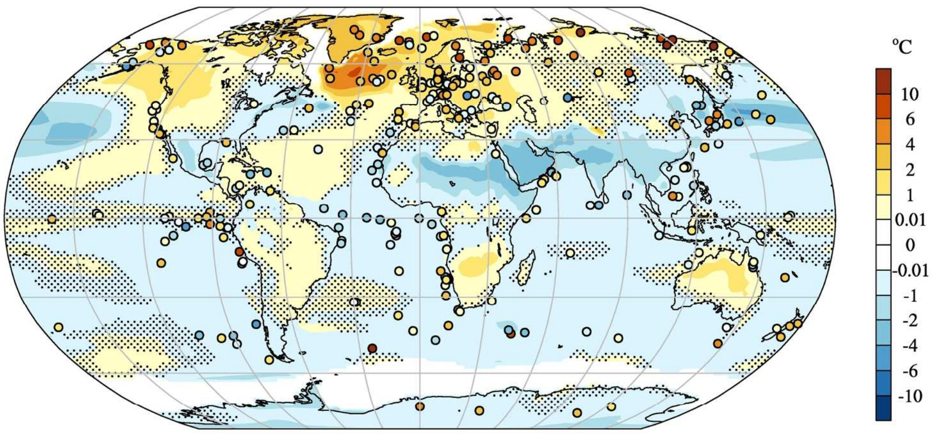

178x178mm (300 x 300 DPI)

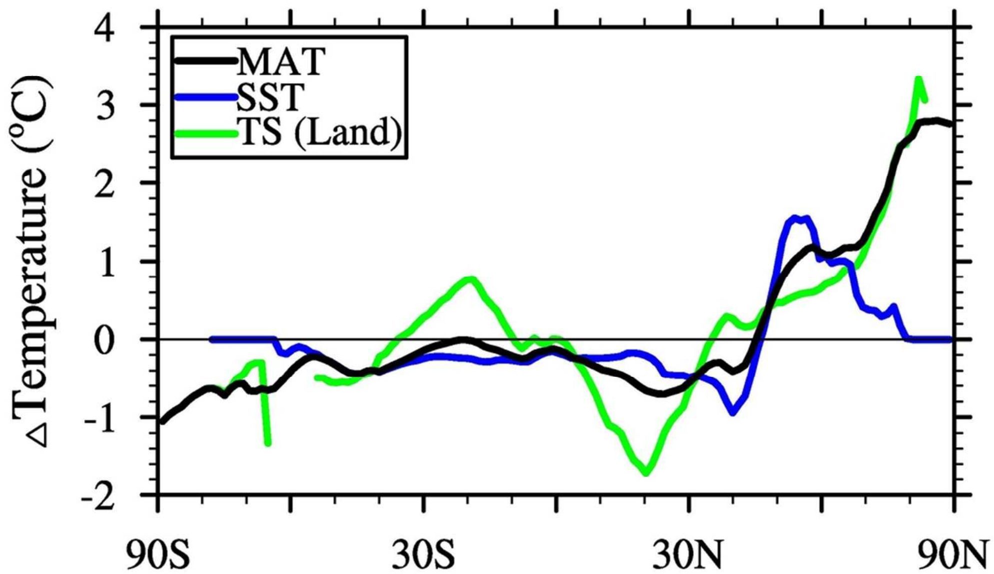

90x90mm (300 x 300 DPI)

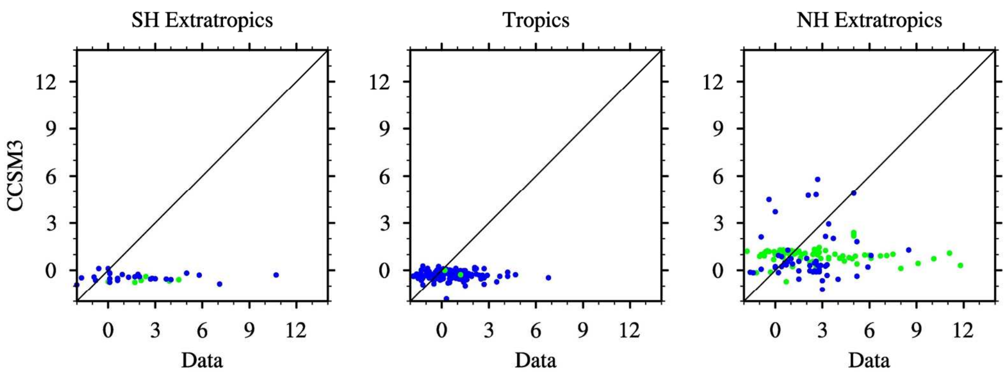

176x176mm (300 x 300 DPI)

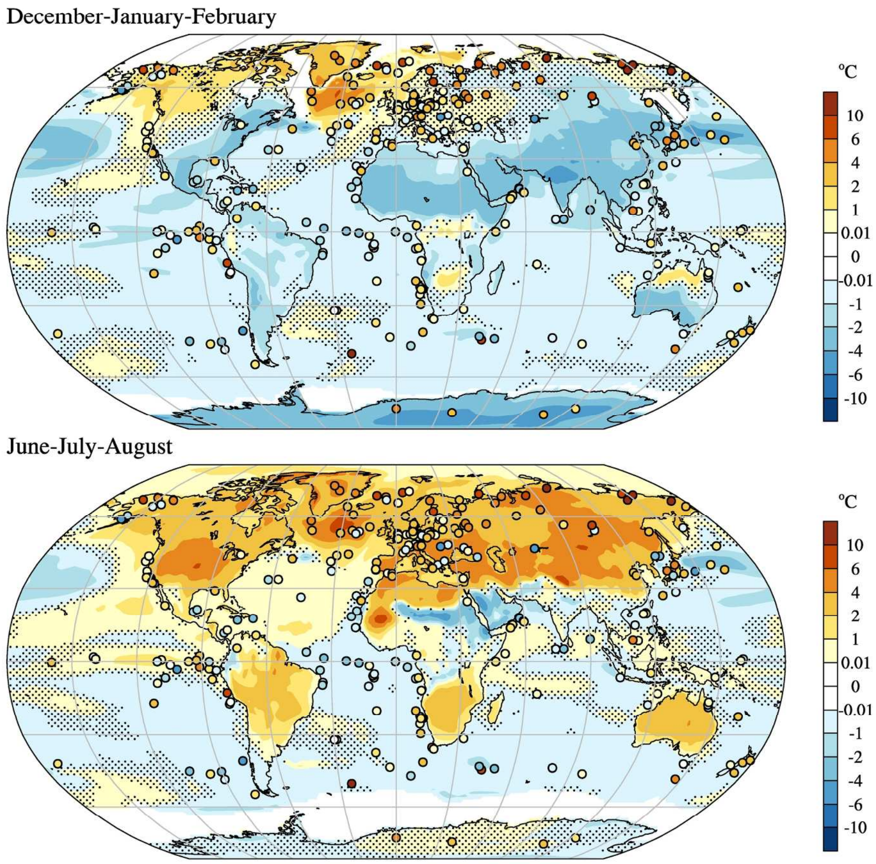

190x190mm (300 x 300 DPI)

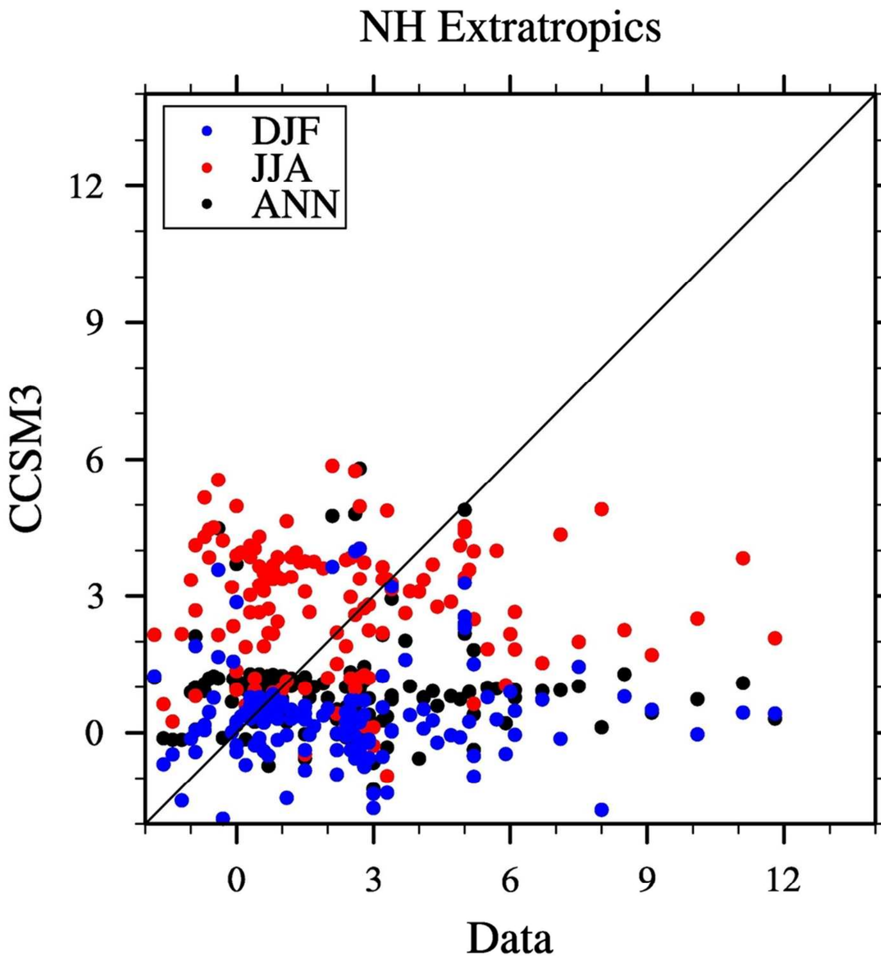

100x100mm (300 x 300 DPI)

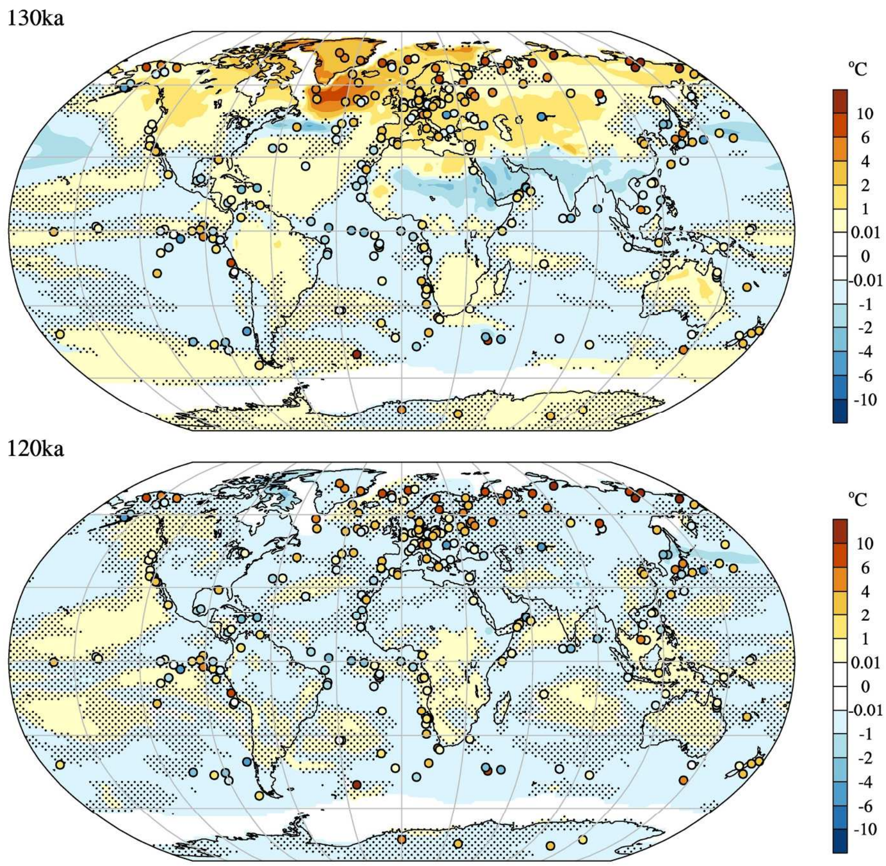

188x188mm (300 x 300 DPI)

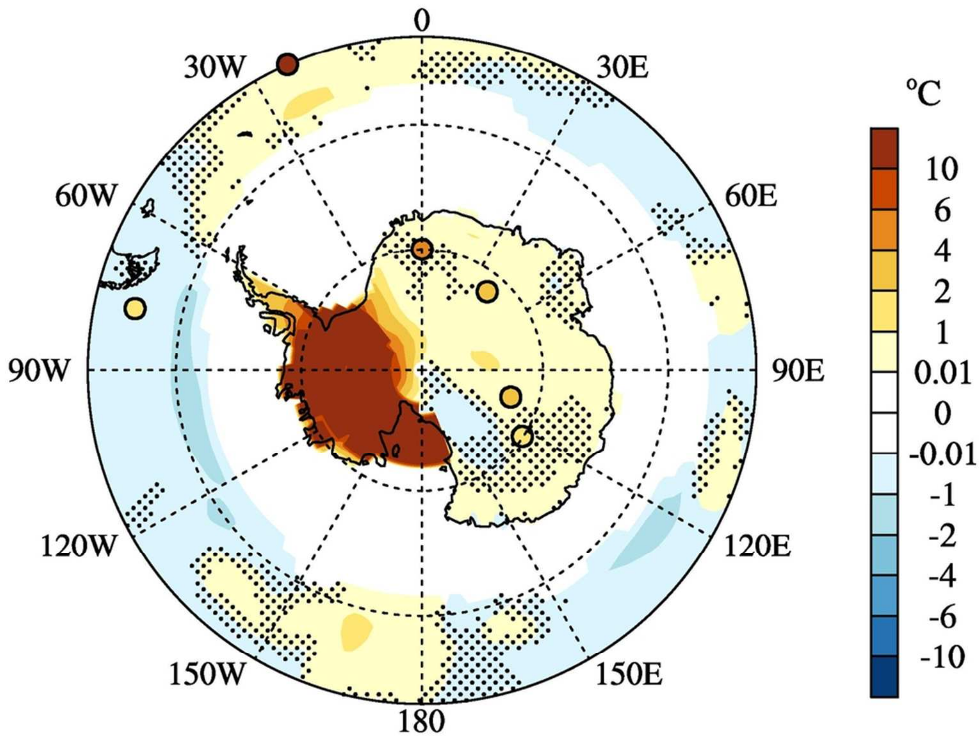

90x90mm (300 x 300 DPI)

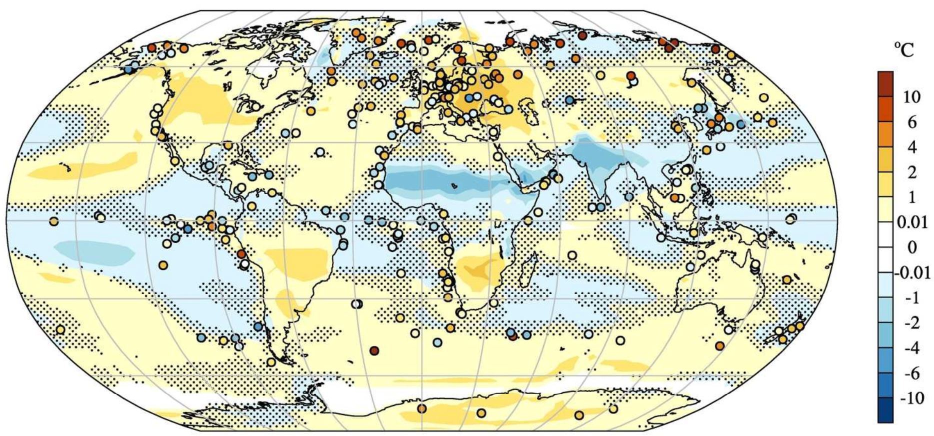

178x178mm (300 x 300 DPI)

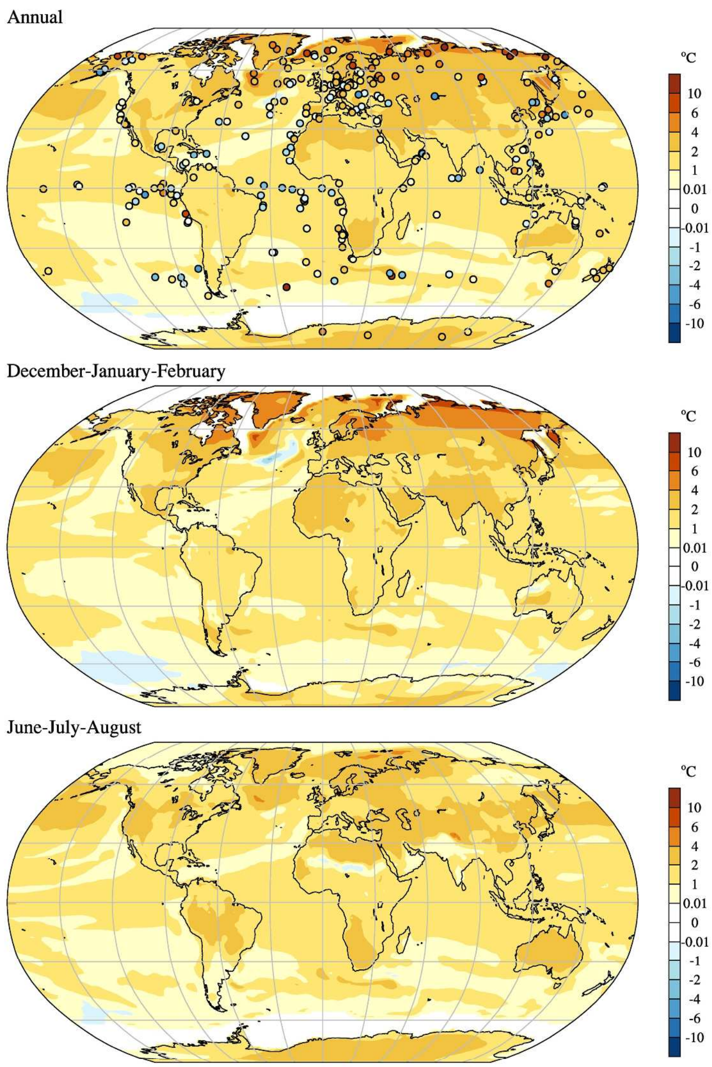

259x312mm (300 x 300 DPI)